energies

MDPI

Article

Impact of Wave-Induced Motion on the Energy Yield Differences Between Offshore Bifacial and Monofacial Photovoltaic Arrays

Aidha Muhammad Ajmal and Yongheng Yang *

College of Electrical Engineering, Zhejiang University, Hangzhou 310027, China; aida.m.khan.1@gmail.com
* Correspondence: yoy@zju.edu.cn

Abstract

Although offshore photovoltaic (PV) systems have attracted increasing interest as a solution to land-use limitations, the influence of offshore-specific dynamic environmental conditions on PV performance remains insufficiently understood. Existing studies have primarily focused on static operating conditions or general energy yield comparisons between bifacial and monofacial PV technologies, while the combined effects of wave-induced motion, module tilt-angle, and sea-surface albedo on offshore PV performance have received limited attention. To address this gap, this study develops a parametric simulation framework to investigate the sensitivity of offshore bifacial photovoltaic (biPV) and monofacial photovoltaic (moPV) arrays to key offshore environmental and operational parameters. Given the scarcity of long-term operational data for offshore PV installations, a hypothetical offshore plant located in the Yellow Sea, China, is considered using real meteorological inputs. In this study, 16 kWp offshore biPV and moPV arrays are modeled and compared in terms of their performance through three case studies examining wave motions, tilt-angle variations, and surface albedo effects. Performance metrics such as maximum irradiance, total energy yield, energy yield losses, wave-induced power loss, and bifacial gain (BG) are analyzed and compared. The findings indicate that increasing wave motion diminishes the total energy yield due to higher tilt-angle fluctuations. Nevertheless, the biPV array regularly outperforms the moPV array because of the effect of the rear-side irradiance. The tilt angle analysis reveals a trade-off between energy yield and BG, with BG increasing from 0.05% to over 10% as the tilt angle increases from 10° to 45°. Higher surface albedo further enhances bifacial performance, increasing BG from 4.5% to 17.8% for albedo values of 0.05 and 0.25, respectively.

Keywords: bifacial PV module; monofacial PV module; offshore application; wave-induced motion; dynamic environmental conditions

Academic Editor: Maria Vicidomini

Received: 15 May 2026
Revised: 21 June 2026
Accepted: 2 July 2026
Published: 3 July 2026

1. Introduction

Renewable energy sources (RESs) play a vital role in meeting the growing global demand for sustainable electricity generation. Among these technologies, photovoltaic (PV) systems have emerged as one of the most promising RESs due to their abundant resource availability, low environmental impact, and relatively simple maintenance requirements. Conventional monofacial photovoltaic (moPV) modules have long dominated the solar market, whereas bifacial photovoltaic (biPV) modules have attracted increasing attention

 https://doi.org/10.3390/en19133170

in recent years. Unlike monofacial modules, biPV technology converts solar radiation incident on both the front and rear surfaces into electrical energy, enabling energy yield improvements of approximately 25–30% under suitable operating conditions [1]. As a result, the global market share of bifacial modules is projected to increase significantly, reaching nearly 70% by 2030, as illustrated in Figure 1 [2].

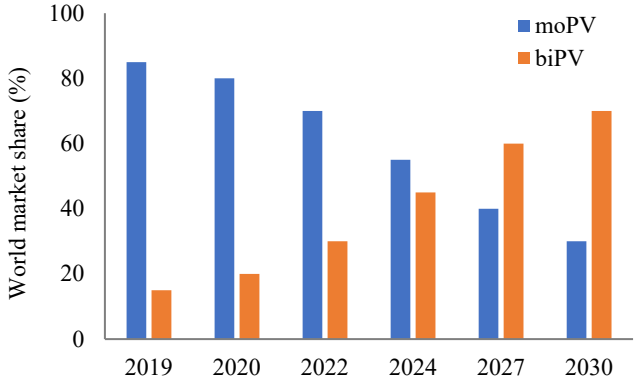

Figure 1. Development trend of bifacial PV technology in markets [2].

Despite the rapid expansion of land-based PV installations, several technical and practical challenges remain. Variations in solar irradiance and ambient temperature caused by changing weather conditions lead to fluctuations in module operating conditions and power output, ultimately affecting system efficiency and increasing the cost of electricity generation [3]. Furthermore, utility-scale PV plants require large areas of available land, which are becoming increasingly scarce because of urbanization and population growth [4]. To overcome these limitations, researchers and industry have increasingly explored the deployment of PV systems on water bodies. Offshore floating PV installations utilize vast ocean areas by mounting PV arrays on floating platforms, thereby reducing land requirements while providing access to additional reflected solar radiation from the water surface. This configuration is particularly advantageous for bifacial PV modules, whose rear surfaces can effectively harvest reflected irradiance to enhance overall energy production. Consequently, floating and offshore PV systems have gained considerable attention worldwide because of their relatively straightforward installation, lower deployment costs, simplified maintenance, and improved power generation performance [5].

In offshore environments, water and wind cooling from the sea surface helps enhance the efficiency of PV modules. The findings of a study conducted in [6] indicated that the operating temperature of PV modules installed on water surfaces has been 5 °C lower than that of those installed on land, thereby enhancing the performance of offshore systems [7]. Another study in Singapore found that the operating temperature of floating PV systems is 5 °C to 10 °C lower than similar modules installed on rooftops [8]. Moreover, the wind speeds over open water are higher than land-based, facilitating floating module cooling [9]. The authors in [10] confirmed that increasing the wind speed by 49% reduced the operational temperature of the floating PV system by 11.60% and increased the generated power by 20.28%. However, offshore environments are characterized by harsh conditions, including elevated humidity, high salinity, and strong wave motions, which significantly impact the performance and lifespan of PV modules [11]. Wave motions cause movements in the floating structures that hold the PV panels. These movements change the orientation of the PV panels and tilt them away from their initial setting, thereby altering the amount of incident irradiance on these panels, resulting in electrical mismatch power losses [12].

Several studies have investigated the impact of wave-induced motion on the performance of offshore PV systems. Reported power losses vary considerably because they depend on factors such as platform design, sea state, environmental conditions, and the modeling or measurement approach employed. A comprehensive study presented in [13] found that wave-induced power losses ranged from 0.4% to 15% based on the floating structure, simulation approach, and operational conditions. In 2024, an experimental investigation on catamaran-based floating PV modules helped to build empirical models that describe the impact of wave motion on system performance. However, comprehensive studies that simultaneously consider wave motion, wind loading, mooring dynamics, and thermal effects remain limited [14]. In 2021, DNV Global developed a study to assess mismatch power losses considering platform tilt and azimuth angle conditions [15]. In addition, the authors in [16] simulated the performance of ground-based and offshore PV plants, considering the combined influence of wave motion, wind speed, and relative humidity. The results showed that the offshore PV systems produced approximately 13% more annual energy than comparable ground-based applications. Furthermore, the authors in [17] investigated the influence of wave-induced motion on irradiance levels of floating moPV modules and discovered that pitch motion had the highest impact, resulting in irradiance decreases of up to 2.52%. Another study [18] looked at the effect of irradiance fluctuations caused by wave motion on inverter performance and found that inverter efficiency dropped by about 2% under wave conditions. In another study [8], the authors assessed the performance of floating and rooftop PV modules using experimental data gathered in Singapore. Although the outcomes show useful empirical data, laboratory and field-based methodologies are impractical for the preliminary design and predicting the performance of offshore PV modules. Meanwhile, the authors in [19] examined the performance and generated power of a PV system installed on a lake under steady-state conditions using PVsyst 7.0 software. Similarly, the authors of [20] used the System Advisor Model (SAM) to evaluate the power production capacity of a reservoir floating PV array in Brazil, taking into account a fixed moPV array and a constant temperature reduction of 5% compared to land-based PV systems. In [21], the authors proposed a novel electrical model that focuses on the temperature differential induced by water to compare the generated power of floating and ground-based PV plants.

With the widespread adoption of biPV cell technology, interest in assessing its performance has grown, especially under offshore environmental conditions. However, the majority of previous investigations into moPV and biPV systems have been carried out at land-based stations. Understanding the performance of offshore biPV modules under dynamic conditions requires a comprehensive understanding of electrical settings, solar irradiance, solar angles, temperature, and wave motion models. In [22], the authors examined the electrical performance model of land-based moPV modules, and the results confirmed that sequential operation of each sub-model can predict module output. The outcomes of a study published in [23] revealed that moPV and biPV modules are compatible under clear sky conditions. Thermal behavior significantly affects the performance of PV modules, as temperature fluctuations greatly affect their efficiency and longevity. The authors in [24] comprehensively examined the steady-state operating temperature of biPV modules. The authors observed that biPV modules exhibit distinct thermal dynamics compared to moPV modules due to their dual-sided exposure. The results showed that the working temperatures of the biPV modules were 41.5 °C for water surfaces, 44.7 °C for cement, and 43.2 °C for grass. In [25], the authors introduced the concept of a floating biPV system and evaluated its performance in comparison to an established simulated floating moPV system in Water Works, Chandigarh. The outcomes demonstrate that the floating biPV system provides higher power with a performance ratio of 92.9%, superior to the moPV system. In [26], the authors demonstrated that the water surface offers evaporation

cooling, resulting in a lower operating temperature of PV modules and enhancing the produced power by 5–10% under similar irradiance conditions, while the water reflection boosts rear-side irradiance of biPV modules, achieving a performance ratio of up to 87.34%. A study in [27] investigated a floating biPV system using several water coolants. Fresh water showed the best overall performance, yielding the highest power output, performance ratio, and efficiency, as well as the lowest levelized cost of energy and superior environmental results. In [28], floating biPV and moPV modules were tested for seven months in landscape and portrait layouts. The findings showed that the landscape layout of biPV modules resulted in lower operating temperatures and enhanced power output of 3% compared to moPV modules at 2.8%.

In [29], the authors examined the performance of south- and east–west-oriented floating biPV modules. The findings demonstrated that the floating PV system significantly lowers peak power demand and enhances output power, resulting in a BG ranging from 17.87 to 36.08%. A study in [30] indicated that the floating biPV system in a tropical region contributes energy to the grid with a BG of 6.75%. Furthermore, several studies have examined the impact of temperature on the cooling and heat transfer of floating biPV installations across two different climatic zones [31]. A simulation study for land-based and floating applications of moPV and biPV systems, using the experimental data of a plant installed at the "Enel Innovation Lab" in Catania, Italy, was implemented in [32]. The simulation results identified the heat exchange coefficients of the software's thermal models and confirmed that the albedo is a sensitive factor for the biPV modules. In [33], the authors carried out a comparative analysis of generated power by simulating different PV systems to determine the capacity factor (CF) and bifacial gain (BG), as well as monthly and annual energy yield metrics. The authors elucidated that the BG of ground-based and floating biPV modules was 2.51% and 4.57%, respectively.

In [34], the authors investigated the impact of constant and dynamic albedo on the energy generation of an offshore PV system deployed in the North Sea. The findings indicated that dynamic albedo improves system performance by up to 3.04% over constant albedo. However, the albedo for an open ocean is determined by atmospheric and oceanic characteristics; solar zenith angle; ocean surface roughness, which is affected by wind speed; and solar irradiance [35]. For comparison, typical albedo values vary from 0.03 to 0.10 for open ocean water, 0.15–0.25 for vegetation, 0.30–0.45 for dry sand, 0.50–0.70 for sea ice, and 0.80–0.95 for fresh snow [36]. These values highlight the relatively low reflectivity of open-water surfaces compared with many land-based and cryospheric environments. Whitecaps generated by breaking waves exhibit a higher effective reflectance, with reported values of approximately 0.22 in the visible spectrum, considerably exceeding that of calm water surfaces. As a result, wave-induced whitecap formation may increase the reflected irradiance available to the rear side of biPV modules [37]. The studies have demonstrated that horizontal floating PV systems can achieve improved performance under dynamically varying albedo conditions. However, the panel tilt in such systems is generally limited to 20°, and as shown in [16], tilt angles exceed 10° only under high wind-speed conditions. Consequently, the contribution of reflected solar irradiance to horizontally mounted PV panels remains relatively small. In contrast, floating PV systems installed with a permanent non-zero tilt angle are expected to derive greater benefits from incorporating dynamic albedo effects into performance assessments.

Despite the growing interest in offshore PV systems, several important knowledge gaps remain regarding their performance under offshore-specific dynamic operating conditions. Previous studies have primarily focused on static operating conditions, overall energy yield assessments, or general comparisons between biPV and moPV technologies. However, the combined influence of wave-induced motion, module tilt-angle variation, and sea-surface albedo on the performance of offshore PV systems has not been system-

atically investigated. As offshore environments are characterized by continuous platform motion and varying reflective conditions, a better understanding of how these factors affect irradiance collection, energy yield, and bifacial gain is essential for the design and optimization of offshore PV installations.

To address this gap, this study develops a dynamic offshore PV simulation framework and performs a parametric investigation of a hypothetical 16 kWp offshore PV system located in the Yellow Sea, China, using real meteorological data. Three case studies are conducted to evaluate the effects of wave motion conditions, module tilt-angle variations, and sea-surface albedo on the performance of biPV and moPV arrays. Key performance indicators, including maximum irradiance, total energy yield (E_{yield}), energy yield losses (E_{yield_loss}), wave-induced power loss (W_{P_loss}), and bifacial gain (BG), are analyzed and compared. The main contributions of this work are: (i) quantifying the impact of wave-induced motion on offshore PV performance under different sea states; (ii) assessing the sensitivity of bifacial gain and energy yield to module tilt-angle variations; (iii) evaluating the influence of sea-surface albedo on rear-side irradiance collection and bifacial performance; and (iv) providing design-oriented insights for the optimization of offshore biPV systems operating under dynamic environmental conditions. The organization of the reset of this paper is introduced as follows. In Section 2, the offshore biPV system and wave motion influences, besides the position of the solar angles, as well as the formulation of various models, are discussed in detail. Section 3 presents the system setup, the climatic factors of the offshore environment, and the performance analysis results of various case studies. Finally, concluding remarks are given in Section 4.

2. Offshore PV Systems

Offshore PV systems are an emerging application of floating solar technology specifically developed for deployment in marine environments. Although their overall configuration is comparable to that of conventional land-based PV systems, they differ primarily in that the PV modules are installed on buoyant platforms rather than fixed foundations, as shown in Figure 2. These floating platforms are typically fabricated from high-density polyethylene (HDPE) or fiber-reinforced plastic (FRP) because of their excellent buoyancy, durability, and resistance to the corrosive marine environment. The PV modules are mounted on structural support frames that distribute their weight and transfer loads to the floating platform. Electrical components, including inverters and power converters, are integrated to convert and manage the generated electricity. In addition, mooring and anchoring systems are employed to maintain the platform's position and orientation while limiting drift and excessive movement caused by environmental forces such as waves and currents [38,39].

An offshore moPV installation in the Dutch North Sea has recently been assessed by researchers from the Copernicus Institute at Utrecht University. The outcomes validated the technical feasibility and future scalability of offshore solar technology, with an estimated development to around 100 MW by 2030 and 500 MW by 2035. These estimates are supported by the operational benefits and competitive performance of offshore PV compared with conventional land-based installations [40]. Despite these promising prospects, offshore PV systems operate under continuously changing marine conditions, including fluctuations in wind, waves, and ambient temperature. A comparative investigation presented in [41] showed that wind loading is generally the dominant factor for floating PV installations on sheltered inland waters, whereas wave-induced forces become the primary load in offshore environments, contributing nearly 50% of the total structural loading. Consequently, offshore PV platforms require robust floating structures together with reliable mooring systems capable of withstanding severe ocean conditions. Nevertheless, the surrounding water provides a natural cooling effect that helps maintain lower operat-

ing temperatures than those typically observed in ground-mounted PV systems. Experimental findings reported in [42] confirmed that both floating and offshore PV arrays exhibit reduced module temperatures, which can enhance energy conversion efficiency. Figure 2b presents an example of a pilot offshore PV installation developed by Oceans of Energy in the Dutch North Sea. Under wave action, the floating platform experiences continuous motion, leading to variations in the tilt angle and orientation of the PV modules. These dynamic changes alter the amount of incident solar irradiance received by the modules, resulting in fluctuations and reductions in power generation. The effects of these dynamic behaviors on offshore PV performance are discussed in greater detail in the following sections.

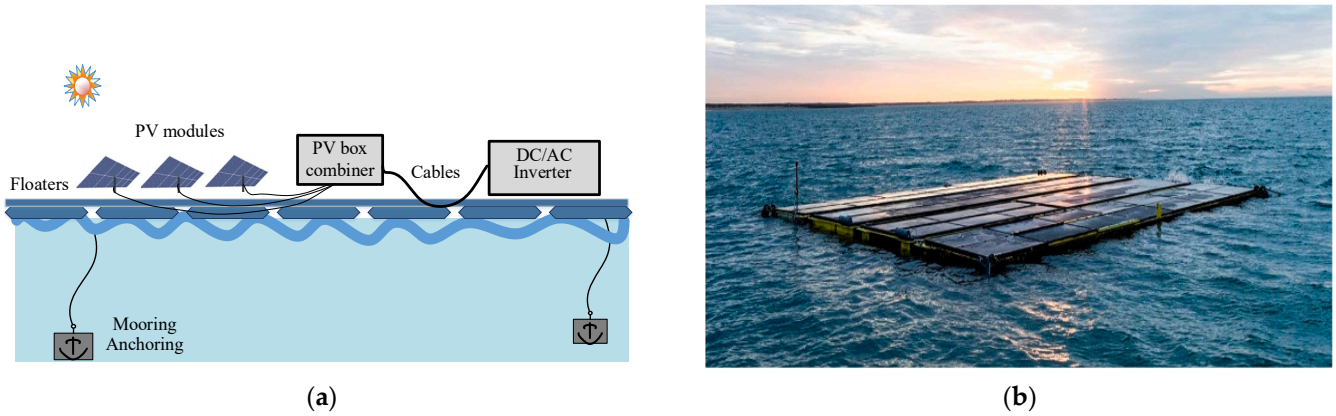

(**a**) (**b**)

Figure 2. (**a**) The main components of an offshore PV system and (**b**) offshore PV system installed in the Dutch North Sea by Oceans of Energy [42].

3. Mathematical Modeling

Figure 3 displays the main models used for modeling offshore biPV modules, consisting of four different model types: electrical, temperature, irradiance, and wave motion models. These models require installation parameters and meteorological data, such as tilt angle, albedo, solar angles, ambient temperature, wind speed, global horizontal irradiance (GHI), direct normal irradiance (DNI), and diffuse horizontal irradiance (DNI). Satellite observations, ground measurement stations, or a combination of both can be used to gather meteorological data. It can also be obtained from databases provided by businesses such as Solargis, NASA, Meteonorm, and the PV Geographical Information System (PVGIS).

In this study, the PV array is assumed to be installed on a pontoon; therefore, both the tilt angle and the orientation are altered across dynamic conditions. The mathematical modeling of the offshore biPV system will be explained as the weather data is converted into critical electrical model parameters by the front and rear irradiance, temperature, wave-induced motion models, tilt angle, and solar angles. At the beginning, the wave-induced motions are modeled under different characteristics over the Yellow Sea. The system is modeled more precisely by evaluating the solar and tilt angles in each time interval based on wave motion conditions. Then, the front and rear irradiance are evaluated based on dynamic changes in the tilt angle of offshore PV modules. Finally, an operating temperature model for PV modules in offshore environments is determined.

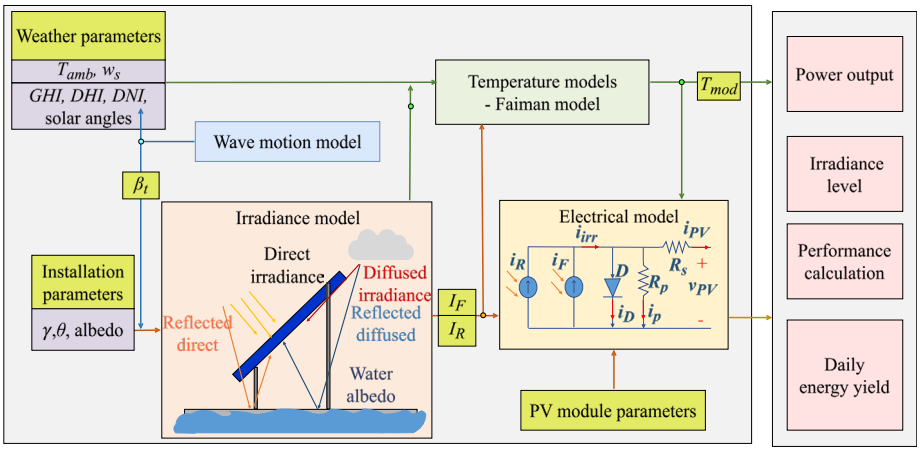

Figure 3. Modeling process of the biPV module.

3.1. Wave Motion Influences

The deployment of PV modules on floating structures results in dynamic motion responses that considerably influence solar irradiance capture and power generation. Therefore, understanding the relationship between wave-induced motion, PV module orientation (tilt and azimuth angles), and the position of the sun is essential for accurately evaluating offshore PV system performance, as direct sunlight exposure maximizes energy yield. In contrast to idealized regular waves, actual ocean conditions are more accurately depicted by non-uniform waves, modeled as a superposition of various uniform wave components characterized by randomized amplitudes, phases, and frequencies. As outlined in [43], the complex wave elevation offers a practical basis for modeling the hydrodynamic forces exerted on floating PV systems [16]. The uniform wave motion can be determined as

$$W(t) = \frac{H_s}{2}\cos\left(\frac{2\pi}{T_p}t + \theta_l\right) \quad (1)$$

where $W(t)$ is the wave motion, H_s is the high of wave motion (m), T_p is the wave period (s), and θ_l is the phase shift angle.

The complex wave motion in the time domain can be expressed as

$$W(t) = \sum_{l=1}^{\infty}\frac{H_s}{2}\cos\left(\frac{2\pi}{T_p}t + \theta_l\right) \quad (2)$$

The tilt angle of the offshore PV panel under wave-induced motion can be expressed as [44]

$$\beta_t = tan^{-1}\left(\frac{\partial W(t)}{\partial t}\right) + \beta_{t0} \quad (3)$$

in which β_t and β_{t0} indicate the tilt angle and the initial tilt angle of the PV module.

The wave model serves as a tool to evaluate the forces acting on offshore PV systems, which in turn influence the dynamic tilt angle (β_t) of the modules' solar zenith angle (θ_s) by wave angle (θ_{wave}). Figure 4 illustrates the impact of wave motions on the tilt angle. From Figure 4a, the initial solar zenith angle (θ_s) is stable when waves are not present. The movement of the wave causes a tilt by θ_{wave}, and thus the solar zenith angle is modified to ($\theta_s + \theta_{wave}$) (see Figure 4b). When the pontoon tilts in the opposite direction, the angle is adjusted to ($\theta_s - \theta_{wave}$) as shown in Figure 4c. Finally, the system returns to stability when the wave goes away, so the solar zenith angle returns to θ_s. In addition, the periodic variation in tilt angle influences the module's effective irradiance, necessitating integration with solar angle models for a comprehensive performance analysis.

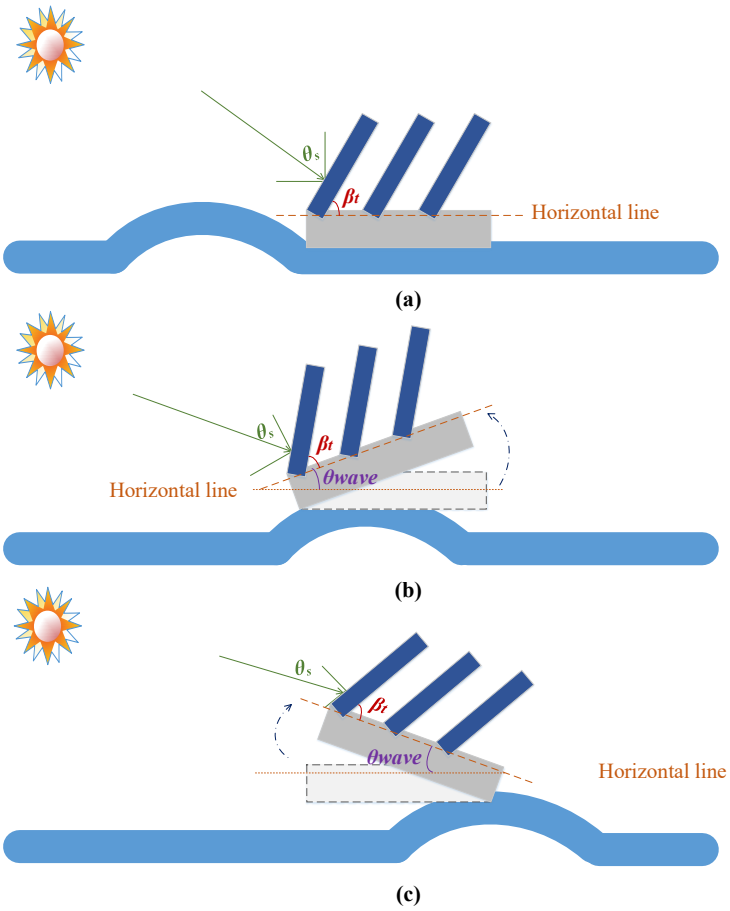

Figure 4. Effect of wave motions on the solar zenith angle and tilt angle of PV modules. (**a**) no wave motion; (**b**) during wave motion; and (**c**) after the wave has passed.

3.2. Position of the Sun and Solar Angle Models

Due to biPV modules receiving solar irradiance from both sides, accurate solar positioning plays an important role in modeling their performance. Solar angles such as the azimuth angle, inclination angle, and zenith angle affect solar irradiance and the power output of PV modules. To model different sun angles, the sun's path relative to the location and orientation of the PV system is taken into account. Figure 5 depicts the various sun angles incident on a tilted PV panel surface. This section covers the major sun angle models.

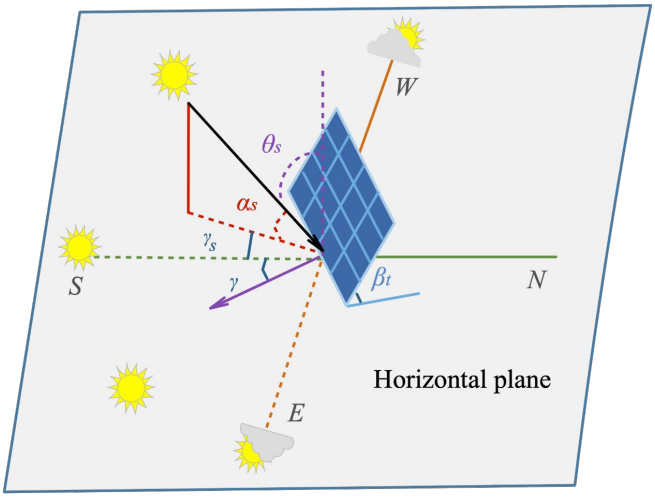

Figure 5. Sun angles over tilted surface, where θ_s, α_s, γ_s, γ, and β_t are the solar zenith, altitude, solar azimuth, PV panel azimuth, and tilt angles, respectively.

Diverse irradiance types, like GHI, DNI, and DHI, are related to the tilt angle and different sun angles, which may be elucidated as [45]:

a. The declination angle (δ) is the angle between the plane through the equator and the earth–sun line (through their center). The solar declination angle is assumed to remain constant during a specific day, while it varies from −23.45° to + 23.45° on 21 December and 21 June, respectively. The solar declination angle may be estimated as

$$\delta^{\circ} = 23.45^{\circ} sin\left[\frac{360(24+n)}{365}\right] \quad (4)$$

where n refers to a Julian day, starting from January 1st.

b. Solar zenith angle (θ_s) is the angle formed by the local vertical (zenith) at a given position on the Earth's surface and the line from that location to the sun's center. It is one of the basic solar geometry properties used to characterize the sun's location in relation to a PV module. It is a significant element in defining the amount of solar irradiance incident on the panel surface, which may be written as

$$\delta^{\circ} = 90^{\circ} - \alpha_s \quad (5)$$

$$\alpha_s = sin^{-1}(cos\delta cosLcos\omega + sin\delta sinL) \quad (6)$$

where α_s is the altitude, L is the latitude, and ω is the solar hour angle, which is determined as

$$\omega = 15(ST - 12) \quad (7)$$

in which ST represents the solar time.

c. Solar azimuth angle (γ_s) is the angle between a line due south and the projection of sun rays on a horizontal plane. Generally, γ_s is negative in the morning, zero at noon, and positive in the afternoon. The solar azimuth angle may be evaluated as

$$\gamma_s = \begin{cases} +sin\omega\left[cos^{-1}\left(\frac{cos\theta_s sinL - sin\delta}{sin\theta_s cosL}\right)\right] & ,\omega > 0 \\ -sin\omega\left[cos^{-1}\left(\frac{cos\theta_s sinL - sin\delta}{sin\theta_s cosL}\right)\right] & ,\omega < 0 \end{cases} \quad (8)$$

d. The angle of incidence (θ) is the angle created between the incoming solar irradiance and the normal perpendicular to the PV module surface. It is an important quantity for estimating the amount of solar irradiance collected by the module, with maximum irradiance occurring when the angle of incidence is zero, which can be computed as

$$\theta = cos^{-1}(cos\theta_s - 12) \quad (9)$$

with γ denoting the azimuth angle of the tilted surface.

3.3. Irradiance on Tilted biPV Panels Models

The irradiance model for a tilted PV module requires meteorological data, specifically GHI, DNI, and DHI, which are the major inputs for estimating irradiance. These data can be obtained from established solar radiation databases, such as SolarGIS and NASA. Based on these parameters, the total solar irradiance incident on the front and back surfaces of a biPV module can be calculated. Figure 6 depicts the component of solar irradiance on the front and back surfaces of a bifacial PV module [46].

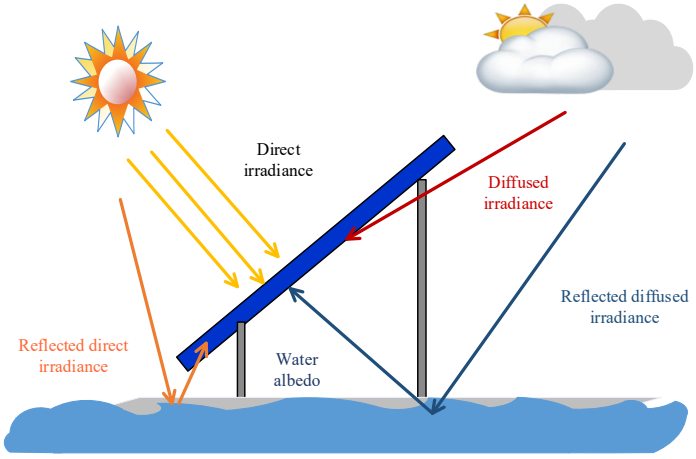

Figure 6. Front and rear-side irradiance components of the biPV module.

3.3.1. Front-Side Irradiance

The front-side irradiance of a tilted PV panel can be obtained by considering the combined contributions of direct beam irradiance, diffuse sky irradiance, and ground-reflected irradiance. The magnitude of each component depends on the solar position, module orientation, tilt angle, and environmental conditions such as albedo. Accordingly, the total front-side irradiance can be evaluated as

$$I_F = I_{F,beam} + I_{F,diff} + I_{F,rgrd} \tag{10}$$

where F refers to the front side and I_{beam}, I_{diff}, I_{rgrd} represent the beam, diffuse, and the ground reflected irradiance, respectively. The beam irradiance is determined as

$$I_{F,beam} = I_{DNI} R_{F,beam} \tag{11}$$

with I_{DNI} being the direct normal irradiance and $R_{F,beam}$ being the ratio of front tilted irradiance and horizontal irradiance, that may be obtained as

$$R_{F,beam} = \begin{cases} \dfrac{cos\theta_F}{cos\theta_{F,s}} & ,\gamma - \dfrac{\pi}{2} \le \omega \le \gamma + \dfrac{\pi}{2} \\ 0 & ,\omega < \gamma - \dfrac{\pi}{2} \quad or \quad \omega > \gamma + \dfrac{\pi}{2} \end{cases} \tag{12}$$

in which γ is the azimuth angle of the PV panel, θ_F is the incident angle, $\theta_{F,s}$ is the front solar zenith angle, and ω is the hour angle. The ground reflected irradiance can be expressed as

$$I_{F,rgrd} = \alpha I_{GHI} V_{F,rgrd} \tag{13}$$

$$V_{F,rgrd} = \left(\frac{1 - cos\beta_t}{2}\right) \tag{14}$$

$$I_{F,diff} = (I_{GHI} - I_{DNI}) V_{F,sky} \tag{15}$$

in which I_{GHI} is the global horizontal irradiance, $V_{F,sky}$ is the view factor of the front side to the sky, $V_{F,rgrd}$ is the view factor of the front side to the ground, and α is the surface albedo.

The diffuse irradiance ($I_{F,diff}$) is more complicated than I_{beam} and I_{rgrd} and it has attracted researchers to develop models such as the Liu and Jordan (LJ) model, HDKR model, and Perez model. The three models of diffused irradiance can be modeled as presented in Table 1.

Table 1. Various diffuse irradiance models. Here, I_0 denotes the extraterrestrial solar irradiance; a and b are the coefficients that account for the effect of the circumsolar incidence angle on the diffuse irradiance of the tilted and horizontal panels; F_1 and F_2 represent the circumsolar brightness coefficient and the horizon brightening coefficient, respectively.

Model	Equation	No.
Liu and Jordan (LJ) model [47]	$I_{F,diff} = (I_{GHI} - I_{DNI})\left(\frac{1-cos\beta_t}{2}\right)$	(16)
HDKR model [37]	$I_{F,diff} = (I_{DHI})\left(\frac{I_{DNI}}{I_0}\right)R_{F,beam} + I_{DHI}\left(1-\frac{I_{DNI}}{I_0}\right)\left(\frac{1-cos\beta_t}{2}\right)\left[1+\sqrt{\frac{I_{DNI}}{I_{GHI}}}sin^3\left(\frac{\beta_t}{2}\right)\right]$	(17)
Perez model [48]	$I_{F,diff} = (I_{GHI} - I_{DNI}) + (1-F_1)\left(\frac{1+cos\beta_t}{2}\right)F_1\frac{a}{b}F_2 sin\beta_t$	(18)

3.3.2. Rear-Side Irradiance

Accordingly, the rear-side irradiance I_R can be obtained as

$$I_R = I_{R,beam} + I_{R,diff} + I_{R,rgrd} = I_{DNI}R_{R,beam} + (I_{GHI} - I_{DNI})V_{R,sky} + \alpha I_{GHI}V_{R,usgrd} + \alpha(I_{GHI} - I_{DNI})V_{R,sgrd} \quad (19)$$

Here, R refers to rear side, $V_{R,sky}$ is the view factor of the rear side to the sky, $V_{R,usgrd}$ is the view factor of the rear *side* to the unshaded ground, $V_{R,sgrd}$ is the view factor of the rear side to the shaded ground, and $R_{R,beam}$ is the ratio of rear tilted irradiance and horizontal irradiance, which can be calculated as

$$R_{F,beam} = \begin{cases} 0 & ,\omega < \gamma - \frac{\pi}{2} \quad or \quad \omega > \gamma + \frac{\pi}{2} \\ \frac{cos\theta_R}{cos\theta_{R,s}} & ,\gamma - \frac{\pi}{2} \le \omega \le \gamma + \frac{\pi}{2} \end{cases} \quad (20)$$

with $\theta_{R,s}$ being the rear solar zenith angle.

The view factor is an important term in estimating the rear-side irradiance. Figure 6 depicts three view factors ($V_{R,sky}$, $V_{R,sgrd}$, and $V_{R,unsgrd}$) for a biPV module based on length (L), elevation (H), and tilt angle (β_t). These factors represent the rear panel's view to the sky, unshaded ground, and shaded ground, respectively. Additional information can be found in [49].

The view factor of the rear side to the sky $V_{R,sky}$ can be calculated as

$$V_{R,sky} = \left(\frac{1-cos\beta_t}{2}\right) \quad (21)$$

The view factor of the rear side to unshaded ground $V_{R,usgrd}$ is expressed as

$$V_{R,usgrd} = V_{R-DQ} + V_{R-CF} \quad (22)$$

where V_{R_DQ} and V_{R_CF} are the view factors of the rear side to the DQ and CF, respectively (see Figure 7), which can be expressed as

$$V_{R-DQ} = \frac{V_{R(OF-DQ)}\overline{OF} - V_{R(AF-DQ)}\overline{AF}}{\overline{OA}} \quad (23)$$

$$V_{R-CF} = \frac{V_{R(OF-CF)}\overline{OF} - V_{R(AF-CF)}\overline{AF}}{\overline{OF}} \quad (24)$$

in which $V_{R(OF\text{-}FQ)}$ is the view factor of the OF to DQ rear side, $V_{R(AF\text{-}FQ)}$ is the view factor of the AF to DQ rear side, $V_{R(OF\_CF)}$ is the view factor of the OF to CF rear side, and $V_{R(AF\_CF)}$ is the view factor of the AF to CF rear side (refer to Figure 7). These can be calculated as

$$V_{R(OF-DQ)} = V_{R(OF-DQ)} - V_{R(OF-FD)} = \frac{1+cos\beta_t}{2} - \frac{\overline{AF+\overline{FD}-\overline{OD}}}{2\overline{OF}} \quad (25)$$

$$V_{R(AF-DQ)} = V_{R(AF-FQ)} - V_{R(OF-FD)} = \frac{1+cos\beta_t}{2} - \frac{\overline{AF+\overline{FD}-\overline{OD}}}{2\overline{AF}} \quad (26)$$

$$V_{R(OF-CF)} = \frac{\overline{OF}+\overline{CF}-\overline{OC}}{2\overline{OF}} \quad (27)$$

$$V_{R(AF-CF)} = \frac{\overline{AF}+\overline{CF}-\overline{AC}}{2\overline{AF}} \quad (28)$$

The view factor of the rear side to shaded ground $V_{R,sgrd}$ is given in [50]:

$$V_{R,sgrd} = \frac{\overline{OC}+\overline{AD}-(\overline{AC}+\overline{OD})}{2\overline{OA}} \quad (29)$$

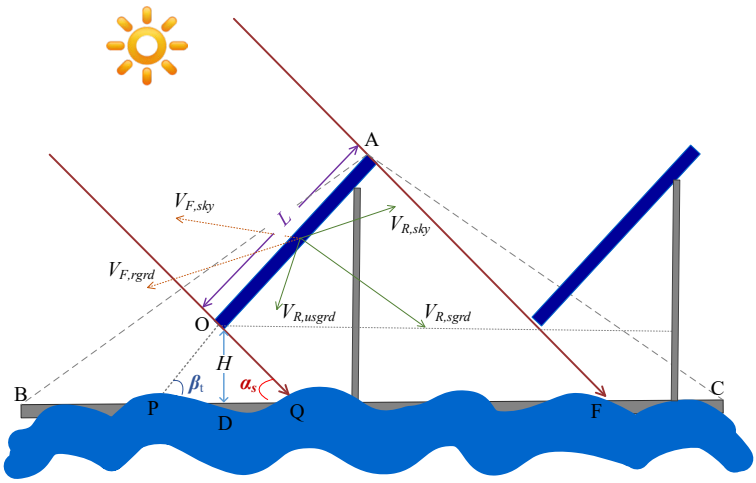

Figure 7. View factors of a biPV module, where $V_{F,sky}$ being the view factor of the front side to the sky, $V_{F,rgrd}$ is the view factor of the front side to the ground, $V_{R,sky}$ being the view factor of the rear side to the sky, $V_{R,usgrd}$ is the view factor of the rear side to the unshaded ground, $V_{R,sgrd}$ is the view factor of the rear side to the shaded ground, L bing the biPV module length, H being the elevation, and β_t being the tilt angle.

3.4. Electrical Model of biPV Module

Accurate electrical modeling of PV modules is required to anticipate the operational characteristics and energy performance of PV systems under changing environmental conditions. In general, biPV modules are designed using the same electrical principles as traditional moPV modules, with the addition of solar irradiance incident on both the front and back surfaces. The irradiance contributions from both sides are integrated using bifaciality coefficients to produce an effective irradiance, which defines the generated photocurrent and acts as the input current source in the corresponding electrical circuit. To represent the electrical behavior of PV modules, several equivalent circuit models have been created, including the single diode model (SDM), double diode model (DDM), and triple diode model (TDM), as presented in Figure 8 [3]. The main difference between these models is their portrayal of semiconductor recombination mechanisms, which affects their accuracy and computational complexity. Among them, the SDM has become the most used model for PV performance analysis because it strikes a good balance between modeling accuracy, computational efficiency, and implementation simplicity while requiring minimal electrical parameters.

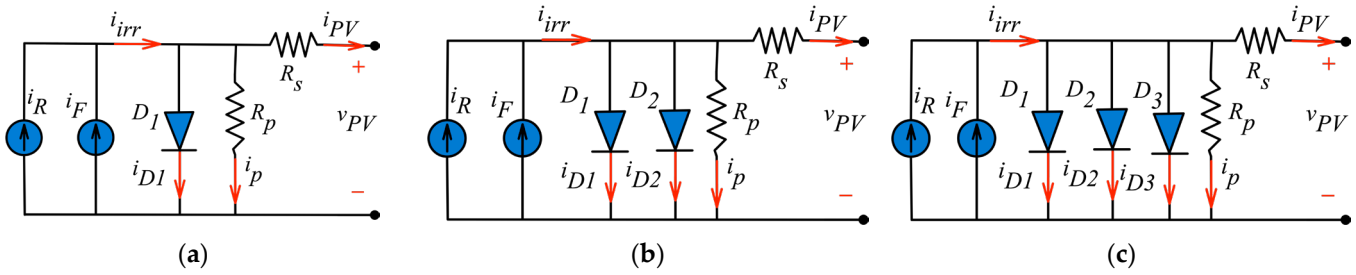

Figure 8. Equivalent circuit of the biPV cell. (**a**) SDM; (**b**) DDM; (**c**) TDM.

In the present study, the electrical behavior of both the moPV and biPV modules is modeled using the SDM. Although offshore deployment introduces dynamic environmental conditions through wave-induced motion, varying irradiance distributions, and changing operating temperatures, these factors primarily influence the environmental inputs to the PV model rather than the intrinsic semiconductor behavior of the solar cells. Consequently, the SDM remains an appropriate and widely validated framework for evaluating the electrical performance of offshore PV systems.

The PV module's outputs are calculated using a well-known equivalent circuit with five parameters of the SDM, which can be represented as

$$i_{PV} = i_{irr} - i_{D1} - i_p = i_F + i_R - i_{01}\left[exp\left(\frac{v_{PV} + i_{PV}R_s}{v_t}\right) - 1\right] - \frac{v_{PV} + i_{PV}R_s}{R_p} \quad (30)$$

where $i_{irr} = i_F + i_R$ represents the total irradiance current while i_F and i_R are the front- and rear-side currents; i_{D1}, i_{01} are the diode current and diode reverse saturation current; i_p is the current via the parallel resistance; R_s is the series resistance; R_p is the parallel resistance; v_t is the diode thermal voltage [$v_t = n_{D1}k_B T_c/q$]; n_{D1} is the diode ideality factor; q is the electronic charge (1.602×10^{-19} C); k_B is Boltzmann's constant (1.381×10^{-23} J/K); and T_c is the solar PV module temperature (°C).

It is clear that five unknown parameters must be examined, including i_{irr}, i_{01}, R_s, R_p, and v_t, which are not available to manufacturers. As a result, parameters must be extracted under standard test circumstances (STCs) first, followed by non-STCs (refer to [51–53]).

3.5. Operating Temperature Model

The operating temperature of biPV modules significantly affects their electrical performance and energy conversion efficiency. In the literature, numerous temperature models have been developed to estimate the cell's operating temperature under various environmental conditions. This subsection reviews the most commonly used temperature models for PV modules.

The Sandia temperature model, which can be achieved as in [54]:

$$T_{mod} = T_{amb} I_T e^{(s_1 + s_2 w_s)} \quad (31)$$

$$T_c = \left(T_{mod} I_T e^{(s_1 + s_2 w_s)}\right) + \frac{I_T}{I_{STC}} \times \Delta T \quad (32)$$

Here, T_c, T_{mod} represents the PV cell and PV module temperature (°C), respectively; T_{amb} represents the ambient temperature (°C); ΔT is the temperature difference between the module and solar cell (°C); I_T and I_{STC} are the total irradiance and irradiance under STCs of the PV module; w_s is the wind speed (m/s); and s_1 and s_2 are empirical parameters that depend on the PV module construction, material properties, and mounting configuration.

The Faiman temperature model is another extensively used approach for calculating PV module operating temperature, particularly in outdoor and marine environments

where solar irradiance and convective heat transfer are important. In this model, the module temperature is given as a function of ambient temperature, incoming solar irradiance, and wind speed [55], which may be defined as

$$T_c = T_{amb} + \frac{\alpha_{bi} I_T \times (1 - \eta_{bi})}{U_0 + U_1 w_s} I_T \quad (33)$$

where α_{bi}, η_{bi} denote the absorptivity and the electrical conversion efficiency of the biPV module, respectively; U_0 (25 W/m^{2}K) represents the overall heat transfer coefficient under zero wind conditions; whereas U_1 (1.2 W/m^3 sK) is the wind-dependent convective heat transfer coefficient that accounts for the cooling effect of airflow over the PV module.

3.6. Energy Yield and Performance Metrics

The total energy yield of the biPV and moPV array is the sum of hourly average power output during the specified time period, assuming that the system works at its maximum power point (MPP). The resulting energy yield is then standardized in relation to the installed peak power, allowing for a consistent comparison of different system configurations. Accordingly, the total energy yield can be represented as

$$E_{bi} = \sum_{t=1}^{n} \frac{P_{MPP,bi}(t)\Delta t}{P_{MPP,bi}} \quad (34)$$

$$E_{mo} = \sum_{t=1}^{n} \frac{P_{MPP,mo}(t)\Delta t}{P_{MPP,mo}} \quad (35)$$

with E_{bi}, E_{mo} being the total energy yield of the biPV and moPV panel (kWh), respectively; and $P_{MPP,bi}$, $P_{MPP,mo}$ being the MPP of biPV and moPV array at time (t).

The bifacial gain (BG) is used to quantify the energy gain of a biPV system in comparison to a moPV system, which is described as

$$BG = \frac{E_{bi} - E_{mo}}{E_{mo}} \times 100\% \quad (36)$$

The wave-induced power loss is determined as the ratio of the difference in total energy yield of the PV array with no wave effect and the total energy yield of the PV array under wave conditions, which can be given as

$$W_{P\_loss} = \frac{E_{ref} - E_{wave}}{E_{ref}} \times 100\% \quad (37)$$

in which W_{P_loss} is the wave-induced power loss, E_{ref} is the reference energy yield of the PV array with no wave, and E_{wave} refers to the energy yield of the PV array under the wave effect.

4. Case Study and Performance Analysis

Since utility-scale offshore PV installations in offshore environments are still at an early stage of development, comprehensive long-term operational and environmental datasets are currently limited. The Yellow Sea, China, was selected as a representative case study due to its growing interest for offshore renewable energy deployment and its relatively shallow coastal waters. However, because large-scale offshore PV projects in this region are still emerging, long-term operational measurements remain scarce. Therefore, this study adopts a parametric simulation approach using real meteorological inputs combined with representative wave and albedo scenarios to systematically investigate the sensitivity of offshore PV performance to these environmental factors.

This study investigates the impact of these parameters on the performance of a 16 kWp offshore moPV and biPV array. The analysis utilizes environmental data collected

from an offshore site in the Yellow Sea, China, located at 38° N and 123° E. The environmental data for the proposed location is obtained from the NASA database, allowing for the extraction of daily, monthly, and yearly datasets that encompass the required environmental parameters for the performance analysis. As illustrated in the coupling framework presented in Section 3 (see Figure 3), the integrated model is implemented in MATLAB/Simulink R2024a. Simulations are conducted to evaluate the system's performance under offshore conditions by altering essential weather and installation parameters. Special focus is directed towards the dynamic impacts of wave motions, which cause continuous variations in module tilt angle and surface albedo, thereby influencing system performance.

Various models of the biPV module incorporate the following inputs:

- Weather parameters: incident irradiance (GHI, DNI, and DHI), ambient temperature, and wind speed, as displayed in Figure 9.
- Installation parameters: tilt angle, sun angles, and albedo.
- PV module specifications: datasheet parameters of the Bi72-445 bifacial module, with the key specifications summarized in Table 2 [56].

Table 2. The biPV and moPV module (BI72-445) specifications [56].

Parameters	Bifacial		Monofacial
	Front Side	Rear Side	
Maximum power (P_{max})	350 W	315 W	350 W
Open circuit voltage (V_{OC})	48.3 V	48.3 V	47.4 V
Short circuit current (I_{SC})	9.53 A	8.58 A	9.64 A
Voltage at MPP (V_{MPP})	38.9 V	38.9 V	38.93 V
Current at MPP (I_{MPP})	9.0 A	8.1 A	9.12 A
Number of cells in a module	72		72
Temperature coefficient of $I_{sc,ref}$	0.0413%/°C		0.044%/°C
Temperature coefficient of $V_{oc,ref}$	−0.29%/°C		−0.29%/°C
Bifacial factor (φ_{bi})	90–95%		

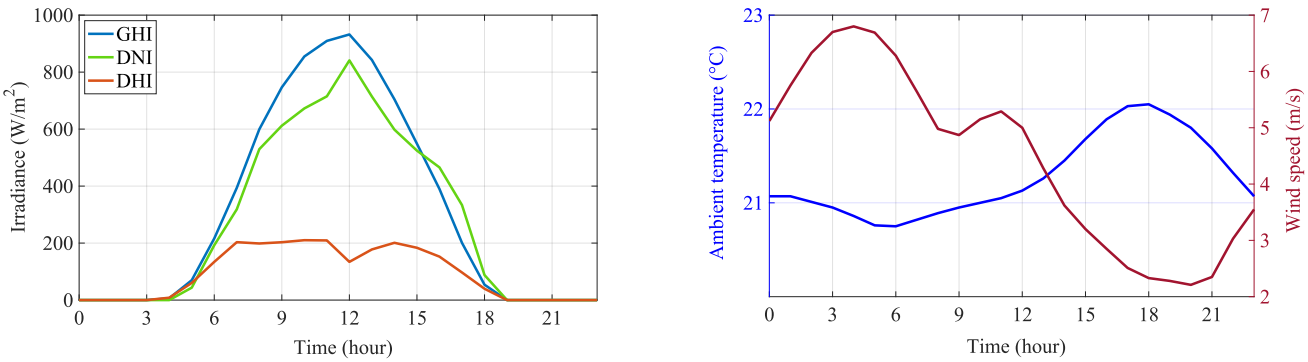

(**a**) (**b**)

Figure 9. Weather dataset for 24 h: (**a**) GHI, DNI, and DHI (W/m²) and (**b**) ambient temperature (°C) and wind speed (m/s).

4.1. Case 1: Different Wave Motion Conditions

To investigate the influence of wave-induced motion on offshore PV performance, four representative wave scenarios were considered. These scenarios were classified as calm, moderate, rough, and severe conditions, corresponding to significant wave heights (H_s) of 0.5, 4, 6, and 8 m and peak wave periods (T_p) of 4, 6, 10, and 12 s, respectively. The selected values were not intended to represent a specific historical record but were chosen

to span a broad range of plausible offshore operating conditions and to facilitate a systematic sensitivity analysis. The adopted significant wave heights encompass both typical and extreme conditions reported for the Yellow Sea in previous wave-climate and offshore engineering studies [57,58]. As wave height and wave period increase, larger platform motions are expected, resulting in greater variations in module orientation and incident solar irradiance. Consequently, these scenarios enable the assessment of offshore PV performance under progressively more challenging dynamic conditions. The analysis was performed for both moPV and biPV arrays using real meteorological inputs. The offshore PV system has an initial module tilt angle of 15°, an azimuth angle of 180° (south-facing), a latitude of 38°N, and a fixed sea-surface albedo of 0.07. For each wave scenario, the dynamic module tilt angle and the corresponding irradiance components were continuously updated throughout the day to account for the effect of wave-induced motion on the incident solar irradiance received by the PV modules.

Figure 10a–d present the generated power and irradiance profiles of the offshore moPV and biPV arrays under different wave motion conditions. Figure 10a,b show that the generated power under calm and moderate wave conditions is relatively similar for both PV technologies. However, the biPV array consistently produces more power than the moPV array due to the additional contribution from rear-side irradiance. Under calm and moderate wave conditions, the biPV array generates approximately 0.4 kW more power than the moPV array. As wave severity increases, the generated power decreases for both technologies because larger wave-induced motions cause greater deviations from the optimum module orientation. Under rough wave conditions, the moPV and biPV arrays achieve maximum power outputs of approximately 7.5 kW and 7.9 kW, respectively, whereas the lowest power outputs are observed under severe wave conditions, reaching approximately 7.3 kW for the moPV array and 7.7 kW for the biPV array.

The irradiance results presented in Figure 10d further explain the observed reduction in power generation. As wave severity increases, the maximum front-side irradiance decreases from 849.4 W/m² under calm conditions to 843.4 W/m², 834.8 W/m², and 822.7 W/m² under moderate, rough, and severe wave conditions, respectively. This reduction is attributed to the larger dynamic tilt-angle variations induced by stronger waves, which increase the deviation of the module surface from the optimum solar incidence angle and consequently reduce the amount of direct irradiance received on the front surface.

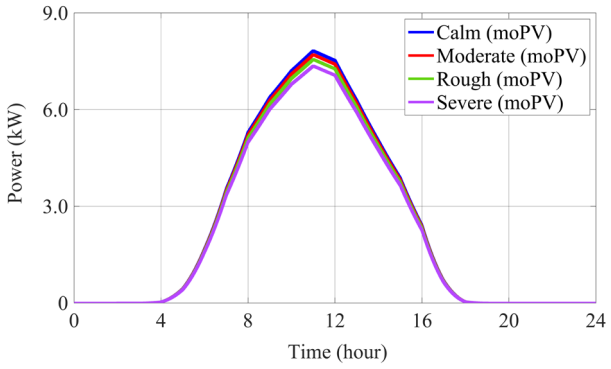

(**a**)

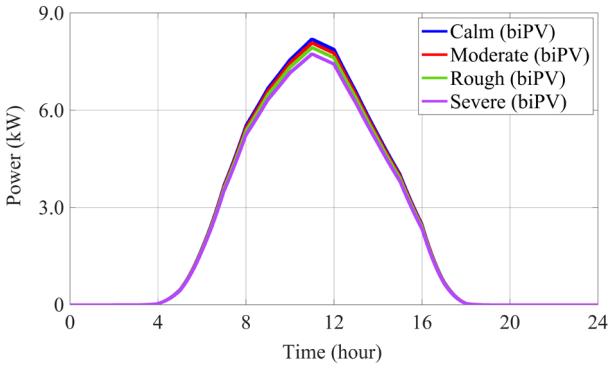

(**b**)

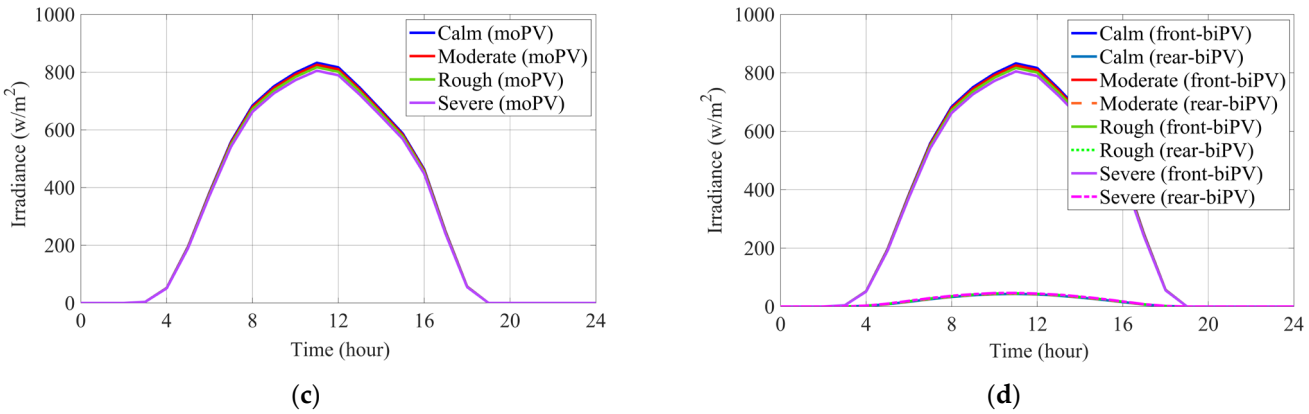

Figure 10. Case 1 results of the offshore PV array under different wave motion conditions: (**a**) the moPV array-generated power (kW), (**b**) the biPV array-generated power (kW), (**c**) the moPV array irradiance (W/m²), and (**d**) the front and rear-side irradiance of the biPV array (W/m²).

In contrast, the maximum rear-side irradiance exhibits an increasing trend with wave severity, rising from 44.8 W/m² under calm conditions to 56.8 W/m², 64.2 W/m², and 73.3 W/m² under moderate, rough, and severe wave conditions, respectively, as illustrated in Figure 11. This behavior is associated with the increased module-angle excursions under rougher sea states, which enhance the exposure of the rear surface to reflected and diffuse irradiance from the sea surface. Although the rear-side irradiance increases by approximately 64% between calm and severe conditions, the reduction in front-side irradiance remains the dominant effect. Consequently, the maximum total irradiance decreases from 880.0 W/m² under calm conditions to 862.2 W/m² under severe conditions, leading to a corresponding reduction in the total energy yield. Nevertheless, the additional rear-side irradiance enables the biPV array to maintain a performance advantage over the moPV array under all investigated wave conditions.

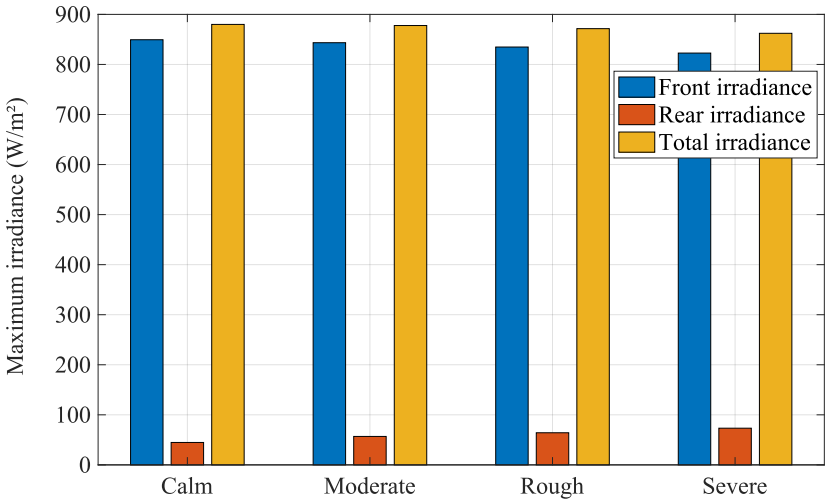

Figure 11. Maximum values of front-side, rear-side, and total irradiance of the biPV array under Case 1.

The performance of the offshore moPV and biPV arrays is significantly affected by wave motion conditions. Figure 12 presents the daily performance estimation under different wave motion conditions, highlighting the benefits of the offshore biPV array. Figure 10 indicates that the biPV array yields greater energy than the moPV array across all wave motion conditions. The biPV array records an energy yield under calm wave conditions

of 60.3 kWh, higher than the moPV array of 57.7 kWh, with a BG of 4.5%, reflecting stable module orientation and reducing the effect of tilt on the rear-side irradiance. The total energy yield of the biPV and moPV arrays diminishes as the wave motion changes from moderate to rough conditions, which is linked to a heightened tilt angle. Consequently, diminishing the effective irradiance of moPV and the front side of biPV modules leads to a modest enhancement in the BG of 4.8% under rough wave motion conditions, due to the rear-side irradiance capture. In severe wave motion conditions, PV modules attain a maximum tilt angle of 45.8°, resulting in an energy yield of 57.1 kWh and 54.4 kWh for the biPV and the moPV arrays, with a peak BG of 5%. This trend highlights the strength of biPV modules in offshore environments, as the input from the rear side contributes to reducing front-side losses caused by wave motion. The results indicate that although extreme wave conditions diminish total energy output, biPV modules exhibit a comparative performance edge over moPV modules, highlighting their appropriateness for offshore PV installations affected by fluctuating wave dynamics.

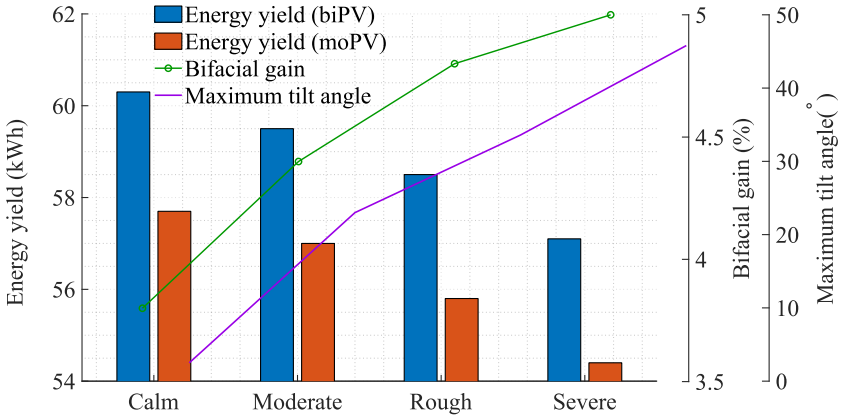

Figure 12. Case 1 performance results of the offshore moPV and the biPV arrays under different wave motion conditions.

4.2. Case 2. Variable Tilt-Angle Conditions

In this case, the generated power of offshore moPV and biPV arrays is examined to determine the impact of various tilt angles. A full-day simulation is carried out utilizing the weather data presented in Figure 9 together with site-specific solar angle calculations for latitude 38°N. The power generation is evaluated at four tilt angles (10°, 25°, 35°, and 45°) under uniform wave-induced motion conditions with H_s = 2 m and T_p = 6 s, while maintaining a constant albedo of 0.07. This case evaluates the potential advantage of dynamic tilt adjustment in offshore contexts and measures the impact on energy production.

Figures 13a and 13b demonstrate the relevant power output curves of the moPV and the biPV arrays in offshore environments across various tilt angles, respectively. From Figure 13, it can be seen that the offshore biPV and the moPV arrays achieve their maximum power of 8.2 kW and 7.8 kW, respectively, at the lowest tilt angle of 10°, while the biPV and the moPV arrays generate a maximum power output of 7.8 kW and 7.3 kW, respectively, when the PV modules are tilted at 25°. Additionally, an increase in the tilt angle from 10° to 35° and 45° results in a more significant reduction in power production. The lowest power production of the biPV and the moPV arrays is 6.2 and 5.6 kW at a tilt angle of 45°. These findings reveal that the biPV array outperforms the moPV array in energy production under different conditions.

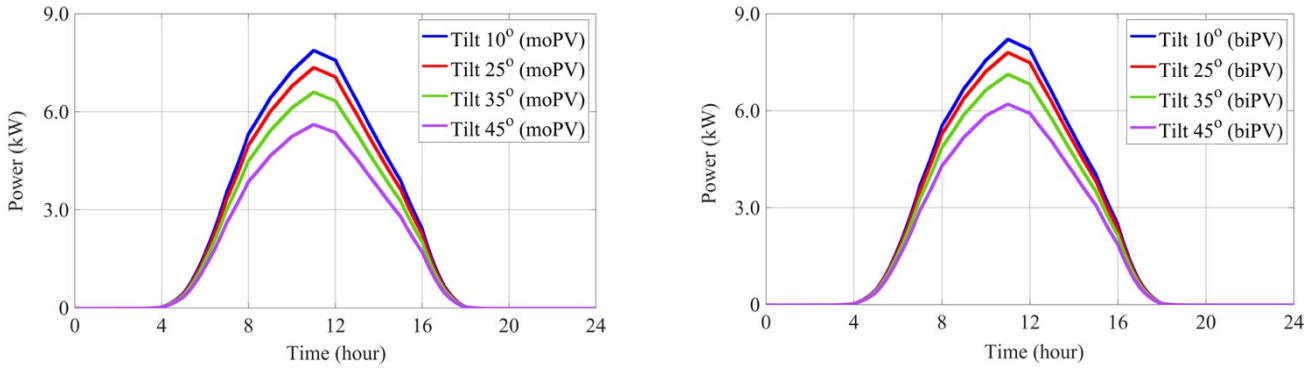

Figure 13. Case 2 results of the generated power of the offshore PV array under various tilt-angle conditions for 24 h: (**a**) the moPV array and (**b**) the biPV array.

The respective total energy yield, which reflects the tilt angle (10°, 25°, 35°, and 45°), as well as the BG of the offshore biPV and moPV arrays, is presented in Figure 14. From Figure 14, it can be observed that the differences in total energy yield among the biPV and moPV arrays, and the BG, increase as the tilt angle increases. The biPV array records the highest energy yield at 60.4 kWh, while the moPV array yields 58 kWh, with the lowest BG value being 0.04% under a tilt angle of 10°. When the tilt angle rises to 25° and 35°, the total energy yield decreases to 57.5 and 53.0 kWh for the biPV array and 54.3 and 49.0 kWh for the moPV array, respectively. This is due to a reduction in the effective irradiance of moPV modules and the front-side irradiance of biPV modules. However, the BG increases to 6.0% and 8.2% because of the effect of the rear-side irradiance from biPV modules. The biPV and the moPV arrays reach the lowest energy yield at 46.4 kWh and 42 kWh, respectively, at the highest tilt angle of 45°. The BG records the maximum value of 10.5%, highlighting the rear-side effect of biPV modules. The outcomes exhibit that the lower tilt angle increases the total energy yield, whereas the higher tilt angle enhances the BG. Optimal offshore PV systems require a balance between the energy yield and the BG, considering the wave motions and structural limitations.

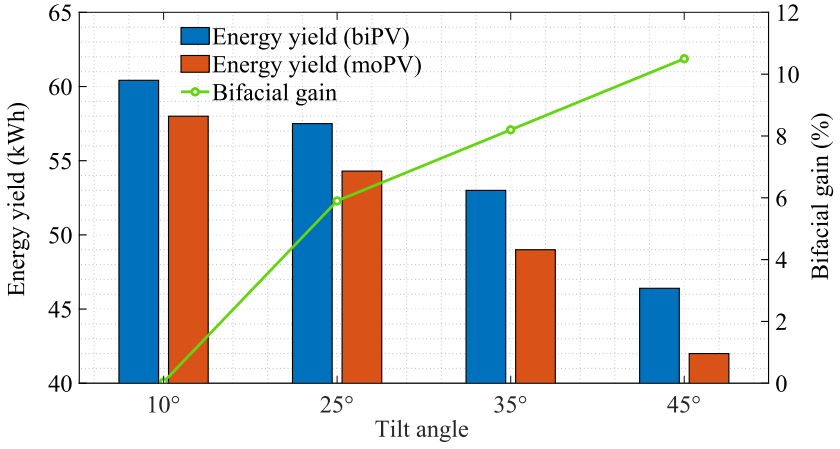

Figure 14. Case 2 performance results of the offshore moPV and the biPV arrays under different tilt-angle conditions.

4.3. Case 3. Affect of Albedo Fluctuations

Different albedo levels are utilized in this case to predict the power generation and energy yield of offshore biPV and moPV arrays over 24 h. PV modules are adjusted at a fixed tilt angle of 15°, 180° facing south, and the latitude is 38°N. Then, the generated

power and irradiance of the biPV and moPV arrays are evaluated across four different albedo levels (0.05, 0.07, 0.15, and 0.25), under wave motion conditions at H_s = 2 m and T_p = 6 s. Both biPV and moPV arrays are simulated utilizing real weather inputs, as illustrated in Figure 9.

Figure 15 presents the irradiance characteristics of the offshore biPV modules under different albedo conditions. As expected, the front-side irradiance remains nearly unchanged across all investigated albedo values because it is primarily determined by the incident solar radiation and module orientation. In contrast, the rear-side irradiance is highly sensitive to surface reflectivity. The maximum rear-side irradiance increases substantially as the albedo rises from 0.05 to 0.25, reaching approximately 185.2 W/m² under the highest albedo condition. This behavior occurs because higher surface reflectivity increases the amount of reflected irradiance incident on the rear surface of the bifacial modules. Consequently, the total irradiance received by the biPV modules increases with albedo, demonstrating the strong dependence of bifacial performance on rear-side irradiance collection.

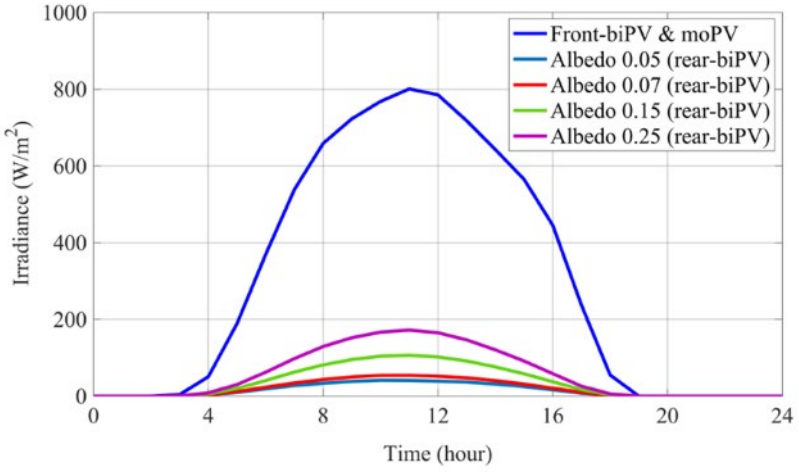

Figure 15. The front-side biPV and moPV modules' irradiance and the rear-side irradiance of biPV modules under albedo fluctuations.

The increase in rear-side irradiance directly affects the generated power of the bifacial modules, as illustrated in Figure 16a,b. The difference in power production between the biPV and moPV arrays becomes increasingly pronounced with increasing albedo. At an albedo of 0.05, the maximum power advantage of the biPV array is approximately 0.33 kW. This difference increases to 0.93 kW and 1.61 kW at albedo values of 0.15 and 0.25, respectively. The enhanced power generation is primarily attributed to the additional rear-side irradiance captured by the bifacial modules, while the moPV array remains largely unaffected by albedo variations because only the front surface contributes to power generation.

https://doi.org/10.3390/en19133170

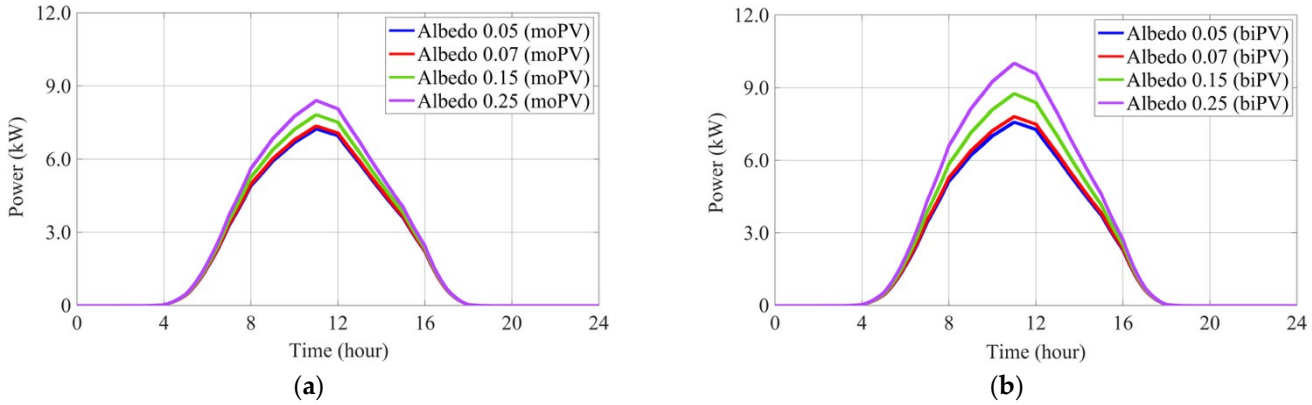

Figure 16. Case 3 results of the generated power of the offshore PV array under albedo fluctuations for 24 h: (**a**) the moPV array and (**b**) the biPV array.

Figure 17 shows the total energy yield of the biPV and the moPV arrays, as well as BG, in offshore environments under albedo fluctuations. In Figure 15, it is evident that the biPV array generates a total energy yield of 56.02 kWh, surpassing the moPV array output of 53.6 kWh, resulting in a modest BG of 4.5% under the lowest albedo value of 0.05. The total energy yield of the biPV and the moPV arrays is slightly increased to 57.5 and 54.3 kWh, respectively, with a BG of 6% across an albedo of 0.07. The biPV array achieves the total energy yields of 63.8 kWh and 72.2 kWh, while the moPV array yields total energy of 57.4 kWh and 61.3 kWh with BG of 11.1% and 17.8% at albedo 0.15 and 0.25, respectively. Such an increase indicates that reflected and diffuse irradiance on the rear side of biPV modules becomes more effective. These outcomes prove that biPV modules are more effective than moPV modules due to their rear-side irradiance under high albedo levels. Overall, this case confirms that the albedo value plays an important role in enhancing the performance of offshore biPV systems, highlighting the importance of surface reflectivity in system design optimization.

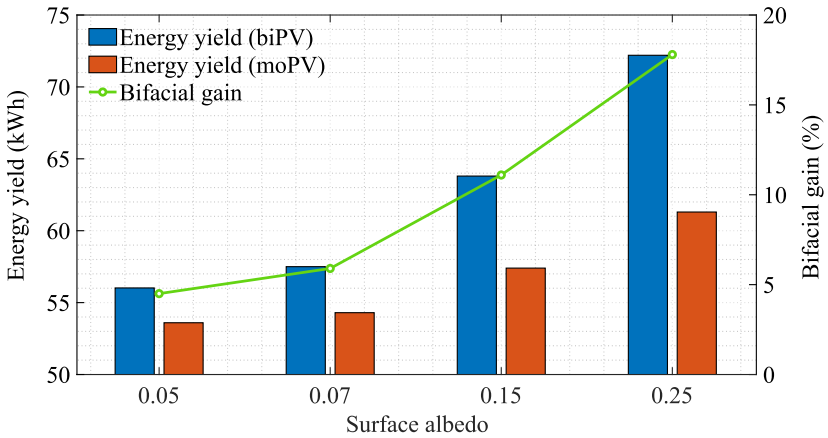

Figure 17. Case 3 performance results of the offshore moPV and the biPV arrays under albedo fluctuations.

4.4. Comparative Analysis

After evaluating the effects of wave-induced motion, module tilt angle, and surface albedo on offshore biPV and moPV arrays, several important observations can be drawn:

- Wave-induced motion significantly influences the irradiance received by offshore PV modules. As wave severity increased from calm conditions (H_s = 0.5 m) to severe conditions (H_s = 8 m), the average dynamic tilt angle increased from approximately

2.5° to 45.8°. Consequently, the maximum front-side irradiance decreased from 849.4 W/m² to 822.7 W/m², leading to reductions in total energy yield for both technologies. The daily energy yield of the biPV array decreased from 60.3 kWh to 57.1 kWh, while the moPV array decreased from 57.7 kWh to 54.4 kWh. These results demonstrate the importance of minimizing excessive platform motion when designing offshore PV systems.

- Although increasing wave motion reduced the front-side irradiance, the maximum rear-side irradiance increased from 44.8 W/m² under calm conditions to 73.3 W/m² under severe conditions. This increase is attributed to the larger wave-induced tilt-angle variations, which improve the exposure of the rear surface to reflected and diffuse irradiance. As a result, the bifacial modules partially compensated for front-side irradiance losses, maintaining the BG between 4.3% and 5.0% under all investigated wave conditions.
- The tilt-angle analysis revealed a trade-off between total energy production and bifacial performance. Lower tilt angles favored higher energy yield because the module surface remained closer to the optimal orientation relative to the sun. In contrast, larger tilt angles enhanced rear-side irradiance collection and increased the bifacial gain from approximately 0.05% at 10° to more than 10% at 45°. Therefore, the selection of the optimal tilt angle should balance overall energy production and bifacial performance.
- The surface albedo was found to be one of the most influential parameters affecting offshore bifacial PV performance. Increasing the albedo from 0.05 to 0.25 substantially increased the rear-side irradiance contribution and enhanced the bifacial gain from approximately 4.5% to 17.8%. This result highlights the strong dependence of bifacial energy production on reflected irradiance and demonstrates the importance of considering local surface reflectivity during offshore PV system design and site assessment.

Overall, the results consistently demonstrate the superior performance of biPV systems compared with moPV systems under all investigated operating conditions. The additional rear-side irradiance collection enables bifacial modules to maintain higher energy yields and improved resilience to offshore environmental variations. These findings confirm that wave-induced motion, module tilt angle, and sea-surface albedo should all be considered during the design and optimization of future offshore PV installations.

Table 3 summarizes the performance analysis of the offshore moPV and biPV arrays across three case studies, considering factors such as the maximum irradiance (W/m²), total energy yield (E_{yield}) (kWh), energy yield losses (E_{yield_loss}) (kWh), wave-induced power loss (W_{P_loss}) (%), and bifacial gain (BG) (%).

Table 3. Summary of the performance analysis of the offshore moPV and biPV arrays under three case studies.

Case Study		Performance Parameters								
		Maximum Total Irradiance (W/m²)		E_{yield} (kWh)		E_{yield_loss} (kWh)		W_{P_loss} (%)		BG (%)
		biPV	moPV	biPV	moPV	biPV	moPV	biPV	moPV	
Reference	No wave	972.2	927.2	75.6	72.7	-	-	-	-	-
Case 1	Calm	880.0	849.0	60.3	58.1	15.3	15.0	20.2	20.6	3.8
	Moderate	877.7	843.4	59.5	57.0	16.1	15.7	21.3	21.6	4.4
	Rough	871.5	834.8	58.5	55.8	17.1	17.0	22.6	23.4	4.8
	Severe	862.2	822.7	57.1	54.4	18.5	18.3	24.5	25.2	5.0
Case 2	Tilt (10°)	884.0	854.4	60.4	58.0	15.2	14.7	20.1	20.2	0.04
	Tilt (25°)	856.8	818.6	57.5	54.3	18.1	18.4	24.0	25.3	6
	Tilt (35°)	813.4	768.2	53.0	49.0	22.6	23.7	30.0	32.6	8.2

	Tilt (45°)	751.4	698.5	46.4	42.0	29.2	30.7	38.6	42.2	10.5
Case 3	**Albedo (0.05)**	845.7	818.0	56.0	53.6	19.6	19.1	26.0	26.3	4.5
	Albedo (0.07)	856.8	818.6	57.5	54.3	18.1	27.4	24.0	37.7	5.9
	Albedo (0.15)	901.5	821.0	63.8	57.4	11.8	15.3	15.6	21.0	11.1
	Albedo (0.25)	957.4	827.5	72.2	61.3	3.4	11.4	4.5	15.7	17.3

5. Conclusions

This study developed a dynamic simulation framework to compare the performance of a 16 kWp offshore biPV array and a moPV array under varying wave motion conditions, module tilt angles, and sea-surface albedo levels. The results demonstrated that wave-induced motion significantly affects offshore PV performance by altering module orientation and reducing front-side irradiance. As wave severity increased, the daily energy yield decreased from 60.3 kWh to 57.1 kWh for the biPV array and from 57.7 kWh to 54.4 kWh for the moPV array. Despite these losses, the biPV system consistently outperformed the moPV system, maintaining a bifacial gain of approximately 4.3–5.0% due to the contribution of rear-side irradiance. The tilt-angle analysis revealed a trade-off between maximizing total energy production and maximizing bifacial gain. Lower tilt angles favored higher energy yield, whereas larger tilt angles enhanced rear-side irradiance collection and increased bifacial gain to more than 10%. In addition, surface albedo was identified as a key parameter affecting bifacial performance, with bifacial gain increasing from approximately 4.5% to 17.8% as albedo increased from 0.05 to 0.25. Overall, the findings confirm the potential of bifacial PV technology for offshore applications and highlight the importance of jointly considering wave-induced motion, module tilt angle, and sea-surface reflectivity during system design and optimization. Since this work represents a parametric simulation study, future research should focus on validating the proposed framework using measured offshore PV data and investigating additional offshore-specific factors, including platform dynamics and module elevation effects.

Author Contributions: Conceptualization, A.M.A.; Methodology, A.M.A.; Validation, A.M.A.; Writing—original draft, A.M.A.; Writing—review & editing, Y.Y.; Supervision, Y.Y. All authors have read and agreed to the published version of the manuscript.

Funding: This research received no external funding.

Data Availability Statement: The original contributions presented in the study are included in the article, further inquiries can be directed to the corresponding author.

Acknowledgments: The author would like to thank the Power Electronics Control and Integration Laboratory (PENCIL) for providing the funds and resources for research work.

Conflicts of Interest: The authors declare no conflicts of interest.

References

1. Catena, M.; Cascone, I.; Carbone, M. *Performance Estimation of Bifacial pv Modules: A Simulation Approach Through Both Physical and Semi-Empirical Math Models and Its Validation Using Real Bifacial Plant Data*; ENEL Green Power S.P.A.: Rome, Italy, 2018; pp. 16–26.
2. Fischer, M.; Woodhouse, M.; Herritsch, S.; Trube, J. International Technology Roadmap for Photovoltaic (ITRPV). VDMA EV. 2021. Available online: https://itrpv.vdma.org/en/ueber-uns (accessed on 4 April 2025).
3. Ajmal, A.M.; Babu, T.S.; Ramachandaramurthy, V.K.; Yousri, D.; Ekanayake, J.B. Static and dynamic reconfiguration approaches for mitigation of partial shading influence in photovoltaic arrays. *Sustain. Energy Technol. Assess.* **2020**, *40*, 100738.
4. Almeida, S.R.M.; Schmitt, R.; Grodsky, S.M.; Flecker, A.S.; Gomes, C.P.; Zhao, L.; Liu, H.; Barros, N.; Kelman, R.; McIntyre, P.B. Floating solar power: Evaluate tradeoffs. *Nature* **2022**, *606*, 246–249.

5. Kumar, N.; Pachauri, R.K.; Kuchhal, P.; Nkenyereye, L. Floating photovoltaic system based electrical power generation study in Indian context. *Renew. Sustain. Energy Rev.* **2025**, *212*, 115442.
6. Lindholm, D.; Selj, J.; Kjeldstad, T.; Fjær, H.; Nysted, V. CFD modelling to derive U-values for floating PV technologies with large water footprint. *Sol. Energy* **2022**, *238*, 238–247.
7. Liu, L.; Wang, Q.; Lin, H.; Li, H.; Sun, Q.; Wennersten, R. Power generation efficiency and prospects of floating photovoltaic systems. *Energy Proc*. **2017**, *105*, 1136–1142.
8. Liu, H.; Krishna, V.; Lun Leung, J.; Reindl, T.; Zhao, L. Field experience and performance analysis of floating PV technologies in the tropics. *Prog. Photovolt. Res. Appl.* **2018**, *26*, 957–967.
9. Water, W.S.M.-*Where Sun Meets Water: Floating Solar Handbook for Practitioners*; World Bank: Washington, DC, USA, 2019.
10. Elminshawy, N.A.; Osama, A.; El-Damhogi, D.; Oterkus, E.; Mohamed, A.M.I. Simulation and experimental performance analysis of partially floating PV system in windy conditions. *Sol. Energy* **2021**, *230*, 1106–1121.
11. Ajmal, A.M.; Yang, Y.; Zhu, Y. Degradation rate analysis of offshore PV module applications considering climatic stresses and salinity effects. *Sol. Energy* **2025**, *295*, 113522.
12. Nysted, V.S.; Stieng, L.E.S.; Kumar, M.; Roosloot, N.; Otnes, G.; Kjeldstad, T.; Selj, J. Modelling wave-induced losses for floating photovoltaics: Impact of design parameters and environmental conditions. *Sol. Energy* **2025**, *287*, 115678.
13. Vasuki, S.S.; Levell, J.; Santbergen, R.; Isabella, O. A technical review on the energy yield estimation of offshore floating photovoltaic systems. *Renew. Sustain. Energy Rev*. **2025**, *216*, 115596.
14. Huang, L.; Yang, Y.; Khojasteh, D.; Ou, B.; Luo, Z. Floating solar power loss due to motions induced by ocean waves: An experimental study. *Ocean Eng*. **2024**, *312*, 118988.
15. DNV, G.L. *Recommended Practice: Design, Development and Operation of Floating Solar Photovoltaic Systems*; DNVGL-RP-0584; DNV GL: Oslo, Norway, 2021.
16. Golroodbari, S.Z.; Van Sark, W. Simulation of performance differences between offshore and land-based photovoltaic systems. *Prog. Photovolt. Res. Appl.* **2020**, *28*, 873–886.
17. Bugeja, R.; Mule'Stagno, L.; Branche, N. The effect of wave response motion on the insolation on offshore photovoltaic installations. *Sol. Energy Adv.* **2021**, *1*, 100008.
18. Alcañiz, A.; Monaco, N.; Isabella, O.; Ziar, H.J.E.C. Offshore floating PV–DC and AC yield analysis considering wave effects. *Energy Convers. Manag.* **2024**, *300*, 117897.
19. Agrawal, K.K.; Jha, S.K.; Mittal, R.K.; Vashishtha, S. Assessment of floating solar PV (FSPV) potential and water conservation: Case study on Rajghat Dam in Uttar Pradesh. *Energy Sustain. Dev*. **2022**, *66*, 287–295.
20. Lopes, M.P.C.; de Andrade Neto, S.; Branco, D.A.C.; de Freitas, M.A.V.; da Silva Fidelis, N. Water-energy nexus: Floating photovoltaic systems promoting water security and energy generation in the semiarid region of Brazil. *J. Clean. Prod*. **2020**, *273*, 122010.
21. Anusuya, K.; Vijayakumar, K. A comparative study of floating and ground-mounted photovoltaic power generation in Indian contexts. *Clean. Energy Syst*. **2024**, *9*, 100140.
22. Riley, D.; Hansen, C.; Stein, J.; Lave, M. A performance model for bifacial PV modules. In *44th Photovoltaic Specialists Conference* (*PVSC*); IEEE: Piscataway, NJ, USA, 2017.
23. Bouchakour, S.; Valencia-Caballero, D.; Luna, A.; Martel, L. Modelling and simulation of bifacial PV production using monofacial electrical models. *Energies* **2021**, *14*, 4224.
24. Zhang, Z.; Wu, M.; Lu, Y.; Xu, C.; Wang, L.; Hu, Y.; Zhang, F. The mathematical and experimental analysis on the steady-state operating temperature of bifacial photovoltaic modules. *Renew. Energy* **2020**, *151*, 434–442.
25. Avasthi, A.; Garg, R.; Mahajan, P. Comparative analysis of bifacial and monofacial floating solar power plants: Performance evaluation and economic analysis. *Iran. J. Sci. Technol. Trans. Mech. Eng.* **2024**, *48*, 2167–2185.
26. Hasan, M.A.; Sutrisno, B.; Faradilla, A.; Kamil, B.; Khairiani, D.; Lande, N.M.; Sibagariang, Y.P.; Sitorus, T.B. Performance Evaluation of Bifacial and Monofacial Floating Photovoltaic Systems: A Case Study under Tropical Conditions. *Results Eng.* **2025**, *29*, 108791.
27. Rathinavel Pandian, G.; Balachandran, G.B.; David, P.W.; Thangaraj, H. Optimization strategies for bifacial floating photovoltaic systems on different water bodies: A 10E performance evaluation. *Proc. Inst. Mech. Eng. Part E J. Process Mech. Eng.* **2024**, *240*, 09544089241281111.
28. Tina, G.M.; Osama, A.; Mannino, G.; Gagliano, A.; Cucuzza, A.V.; Bizzarri, F. Thermal comparison of floating bifacial and monofacial photovoltaic modules considering two laying configurations. *Appl. Energy* **2025**, *389*, 125732.

29. Bhang, B.G.; Hyun, J.H.; Ahn, S.H.; Choi, J.H.; Kim, G.G.; Ahn, H.K. Optimal Design of Bifacial Floating Photovoltaic System with Different Installation Azimuths. *IEEE Access* **2023**, *11*, 1456–1466.
30. Widayat, A.A.; Ma'arif, S.; Syahindra, K.D.; Fauzi, A.F.; Adhi Setiawan, E. Comparison and Optimization of Floating Bifacial and Monofacial Solar PV System in a Tropical Region. In *2020 9th International Conference on Power Science and Engineering (ICPSE)*; IEEE: Piscataway, NJ, USA, 2020; pp. 66–70.
31. Dörenkämper, M.; Wahed, A.; Kumar, A.; de Jong, M.; Kroon, J.; Reindl, T. The cooling effect of floating PV in two different climate zones: A comparison of field test data from the Netherlands and Singapore. *Sol. Energy* **2021**, *219*, 15–23.
32. Tina, G.M.; Bontempo Scavo, F.; Merlo, L.; Bizzarri, F. Comparative analysis of monofacial and bifacial photovoltaic modules for floating power plants. *Appl. Energy* **2021**, *281*, 116084.
33. Cagle, A.E. The land sparing water surface use efficiency, and water surface transformation of floating photovoltaic solar energy installations. *Sustainability* **2020**, *12*, 8154.
34. Mirbagheri Golroodbari, S.Z. The Sun Is Rising over the North Sea: Assessment of Offshore Solar Photovoltaics. Doctoral Dissertation, Utrecht University, Utrecht, The Netherlands, 2021.
35. Jin, Z.; Qiao, Y.; Wang, Y.; Fang, Y.; Yi, W. A new parameterization of spectral and broadband ocean surface albedo. *Opt. Express* **2011**, *19*, 26429–26443.
36. Duffie, J.A.; Beckman, W.A. *Solar Engineering of Thermal Processes*; John Wiley & Sons: Hoboken, NJ, USA, 2013.
37. Séférian, R.; Baek, S.; Boucher, O.; Dufresne, J.L.; Decharme, B.; Saint-Martin, D.; Roehrig, R. An interactive ocean surface albedo scheme (OSAv1. 0): Formulation and evaluation in ARPEGE-Climat (V6. 1) and LMDZ (V5A). *Geosci. Model Dev.* **2018**, *11*, 321–338.
38. Kumar, J.C.R.; Majid, M.A. Floating solar photovoltaic plants in India–a rapid transition to a green energy market and sustainable future. *Energy Environ.* **2023**, *34*, 304–358.
39. Huang, G.; Tang, Y.; Chen, X.; Chen, M.; Jiang, Y. A comprehensive review of floating solar plants and potentials for offshore applications. *Mar. Sci. Eng*. **2023**, *11*, 2064.
40. Bellini, E. Offshore vs. Land-Based Solar, Pv Magazine International–Photovoltaic Markets and Technology. 2020. Available online: https://www.pv-magazine.com/2020/05/13/offshore-vs-land-based-solar/ (accessed on 22 April 2024).
41. Ikhennicheu, M.; Danglade, B.; Pascal, R.; Arramounet, V.; Trébaol, Q.; Gorintin, F. Analytical method for loads determination on floating solar farms in three typicalenvironments. *Sol. Energy* **2021**, *219*, 34–41.
42. Ziar, H.; Prudon, B.; Lin, F.Y.; Roeffen, B.; Heijkoop, D.; Stark, T.; Isabella, O. Innovative floating bifacial photovoltaic solutions for inland water areas. *Prog. Photovolt. Res. Appl.* **2021**, *29*, 725–743.
43. Huld, T.; Amillo, A.; Gracia, M. Estimating PV module performance over large geographical regions: The role of irradiance, air temperature, wind speed and solar spectrum. *Energies* **2015**, *8*, 5159–5181.
44. Bi, C.; Law, A.W.K. Co-locating offshore wind and floating solar farms–Effect of high wind and wave conditions on solar power performance. *Energy* **2023**, *266*, 126437.
45. Awasthi, A.; Shukla, A.K.; SR, M.M.; Dondariya, C.; Shukla, K.N.; Porwal, D.; Richhariya, G. Review on sun tracking technology in solar PV system. *Energy Rep.* **2020**, *6*, 392–405.
46. Ajmal, A.M.; Yang, Y. Degradation Analysis of Offshore Bifacial PV Modules under Multiple Climatic Stressors. In *Applied Power Electronics Conference and Exposition* (*APEC*); IEEE: Piscataway, NJ, USA, 2025; pp. 3024–3029.
47. Liu, B.Y.H.; Jordan, R.C. The long-term average performance of flat-plate solar energy collectors: With design data for the U.S., its outlying possessions and Canada. *Sol. Energy* **1963**, *7*, 53–74.
48. Perez, R.; Stewart, R.; Arbogast, C.; Seals, R.; Scott, J. An anisotropic hourly diffuse radiation model for sloping surfaces: Description, performance validation, site dependency evaluation. *Sol. Energy* **1986**, *36*, 481–497.
49. S¨onmez, F.F.; Ziar, H.; Isabella, O.; Zeman, M. Fast and accurate ray-casting-based view factor estimation method for complex geometries. *Sol. Energy Mater. Sol. Cells* **2019**, *200*, 109934.
50. Appelbaum, J. The role of view factors in solar photovoltaic fields. *Renew. Sustain. Energy Rev*. **2018**, *81*, 161–171.
51. Ma, T.; Gu, W.; Shen, L.; Li, M. An improved and comprehensive mathematical model for solar photovoltaic modules under real operating conditions. *Sol. Energy* **2019**, *184*, 292–304.
52. Bai, J.; Liu, S.; Hao, Y.; Zhang, Z.; Jiang, M.; Zhang, Y. Development of a new compound method to extract the five parameters of PV modules. *Energy Convers. Manag*. **2014**, *79*, 294–303.
53. Lopez-Garcia, J.; Ozkalay, E.; Kenny, R.P.; Pinero-Prieto, L.; Shaw, D.; Pavanello, D.; Sample, T. Implementation of the IEC TS 60904-1-2 measurement methods for bifacial silicon PV devices. *IEEE J. Photovolt.* **2022**, *12*, 787–797.

54. King, D.L.; Boyson, W.E.; Kratochvill, J.A. *Photovoltaic Array Performance Model*; Sandia National Laboratories: Albuquerque, NM, USA, 2004.
55. Faiman, D. Assessing the outdoor operating temperature of photovoltaic modules. *Prog. Photovolt. Res. Appl*. **2008**, *16*, 307–315.
56. Prism Solar Technologies. "Bi72 Bifacial Modules." Bi72 Bifacial Modules. Available online: https://cdn.enfsolar.com/Product/pdf/Crystalline/5a825bac637ab.pdf (accessed on 3 July 2025).
57. Zhai, F.; Li, P.; Song, D. Interannual wave height variability in the Yellow Sea. *J. Oceanogr.* **2019**, *75*, 235.
58. Gao, H.; Shao, Z.; Wu, G.; Li, P. Study of directional declustering for estimating extreme wave heights in the Yellow Sea. *J. Mar. Sci. Eng.* **2020**, *8*, 236.